

## HEAT TREATMENT EFFECTS ON NON-THERMAL SOL-GEL DRIVEN MESOPOROUS $\text{TiO}_2/\text{SiO}_2$

S. Janitabar Darzi<sup>\*1</sup>, A. R. Mahjoub<sup>2</sup>, A. R. Nilchi<sup>1</sup> and S. Rasouli Garmarodi<sup>1</sup>

\* [sjanitabar@aeoi.org.ir](mailto:sjanitabar@aeoi.org.ir)

Received: March 2011

Accepted: November 2011

<sup>1</sup> Nuclear Fuel Cycle Research School, Nuclear Science and Technology Research Institute AEOL, Tehran, Iran.

<sup>2</sup> Faculty of Science, Tarbiat Modares University, Tehran, Iran.

**Abstract:**  $\text{TiO}_2/\text{SiO}_2$  nanocomposite with molar ratio 1:1 was synthesized by a free calcination sol-gel method using titanium tetra chloride and tetraethylorthosilicate as raw materials. In the composite,  $\text{TiO}_2$  nanocrystals are highly dispersed in the amorphous  $\text{SiO}_2$  matrix and the mater showed size quantization effect arising from the presence of extremely small titanium oxide species having a low coordination number. Thermal phase transformation studies of the as-prepared composite were carried out by means of X-ray diffraction (XRD) patterns and thermogravimetry-differential scanning calorimetry (TG-DSC) analyses. The studies showed existence of anatase phase in all the tested temperatures. When temperature exceeds  $400^\circ\text{C}$ , brookite phase was formed beside anatase phase. At  $950^\circ\text{C}$  amorphous silica matrix was transformed to cristobalite and brookite phase disappeared. Finally, small peaks of rutile phase were detectable at  $1100^\circ\text{C}$ .

**Keywords:** composite, mesoporous,  $\text{TiO}_2/\text{SiO}_2$ , cristobalite, anatase, phase transformation

### 1. INTRODUCTION

$\text{TiO}_2$  was shown in the last decade to be the best candidate for photocatalytic applications but its activity is still not high enough to be suitable for commercial application. One major drawback of this semiconductor is recombination of photogenerated charges (electrons and holes). This factor limits the economical application of  $\text{TiO}_2$ . In order to enhance the activity of catalyst, many efforts have been made to modify  $\text{TiO}_2$  [1–2].

There are several crystalline forms of  $\text{TiO}_2$ , anatase, rutile, and brookite, and anatase phase is proved to have higher photocatalytic activity than amorphous and rutile  $\text{TiO}_2$  [3]. Furthermore, only few studies have examined the photocatalytic activity of brookite  $\text{TiO}_2$  [4].

Nanosized and nanoporous  $\text{TiO}_2$  particles show high photocatalytic activity because they have a relatively large surface area per unit mass and volume, which facilitates the diffusion of the surface, generated charge carriers under light irradiation [5, 6].

During the past years, there have been some studies on the photocatalytic activity of  $\text{TiO}_2$  coupled with metal oxides, like  $\text{SnO}_2$ ,  $\text{ZnO}$  and  $\text{WO}_3$  to improve the photocatalytic activity of

$\text{TiO}_2$ . The results showed that coupled semiconductor photocatalysts were a novel approach to achieve a more efficient charge separation, an increased lifetime of the charge carriers, and an enhanced interfacial charge transfer to adsorbed substrates. At the same time, their physical and optical properties are greatly modified [7]. In the case of  $\text{TiO}_2/\text{SiO}_2$ , the addition of  $\text{SiO}_2$  not only reduces the particles size and increases the specific surface area but also enhances the thermal stability of  $\text{TiO}_2$  particles against anatase to rutile phase transformation [8].

Up to now, many methods such as sol-gel, hydrothermal, microemulsion, chemical vapor deposition, inert-gas condensation, and pulsed laser deposition have been established for the synthesis of  $\text{TiO}_2$  with a certain crystalline phase. Among these preparation techniques, the relatively simple sol-gel method is the most widely used [9]. Sol-gel derived  $\text{TiO}_2$  powders have been reported to show high catalytic activity due to their fine structure, large surface area and high porosity [10]. Unfortunately, the sol-gel-derived precipitates are usually amorphous in nature, which requires further heat treatment to induce crystallization [9].

In the present study, a series of  $\text{TiO}_2/\text{SiO}_2$  nanocomposites were synthesized by sol-gel method and producing of anatase/ $\text{SiO}_2$  nanocomposite was achieved at room temperature under atmospheric pressure.

## 2. EXPERIMENTAL PROCEDURE

### 2. 1. Materials

Titanium (IV) chloride (Fluka), tetraethylorthosilicate (Merck), nitric acid (Merck), and ammonium hydroxide (Fluka) were used as the starting materials without further purification.

### 2. 2. Preparation Of $\text{TiO}_2\text{-SiO}_2$ Composite

For  $\text{TiO}_2\text{-SiO}_2$  preparation,  $\text{TiCl}_4$  was added drop wise to deionised water under vigorous stirring in an ice water bath. The hydrolysis reaction was highly exothermic and HCl was released. The produced dispersion was treated with  $\text{NH}_4\text{OH}$  and pH was adjusted to 7. The resulting solid was collected by filtration and washed with distilled water in order to remove chlorine ions the precipitate was dispersed in 200 ml of 0.3 mol/L  $\text{HNO}_3$ . The mixture was refluxed under vigorous stirring at  $70^\circ\text{C}$  for 16h as Titania sol was prepared. Then, 25ml of tetraethylorthosilicate was added drop wise to the above sol and stirred at  $70^\circ\text{C}$ . The resulting powder was filtered and washed with ultra pure water and then dried at room temperature. The prepared composite was denoted as TSR. The composite powder calcined for 1 h at 400, 600, 800, 950 and  $1100^\circ\text{C}$  with a heating rate of  $10^\circ\text{C}/\text{min}$ . The obtained samples were denoted as TS400, TS600, TS800, TS950 and TS1100.

### 2. 3. Instruments

Percent of each component of composite was determined by X-ray fluorescence (XRF) spectroscopy using Oxford ED 2000. The FTIR spectrum was recorded with a Bruker Vector 22 spectrophotometer. Powder X-ray diffraction (XRD) was used for monitoring the phase composition of the samples and the average crystallite sizes of synthesized sample was determined by employing the Scherrer equation,  $D$

$= 0.9 \lambda / (\beta \cos \theta)$ , where  $D$  is the average crystallite size (nm),  $\lambda$  is the applied X-ray wavelength ( $\lambda=1.5406 \text{ \AA}$ ),  $\theta$  is the diffraction angle and  $\beta$  is a full-width at half the maximum of diffraction line observed (observed  $2\theta=25.6$  in radians [11]). Thermogravimetry analysis and differential scanning calorimetry (TGA–DSC) were carried out using STA 1500 Rheometric Scientific Unit. Transmission electron micrographs were taken with a transmission electron microscope (Philips EM208S). The microstructure of the product was studied by scanning electron microscopy (SEM, Philips XL30). Spectroscopic analysis of  $\text{TiO}_2$  was performed using UV-vis spectrophotometer (Shimadzu UV 2100). The Brunauer–Emmett–Teller specific surface area and Barret–Joyner–Halenda pore size distribution of the sample were determined through nitrogen adsorption isotherms with a Quantachrome NOVA 2200e system (Hook, UK).

## 3. RESULTS

The chemical composition of the as-prepared nanocomposite was determined by X-ray fluorescence (XRF) technique, and the result is listed in Table 1.

According to Fourier transform infrared spectroscopy (FT-IR) analysis of as-prepared  $\text{TiO}_2/\text{SiO}_2$  sample (Figure 1), there are three characteristic bands at around 1100, 950, and 490

**Table 1.** Chemical compositions of the as-prepared nanocomposite determined by XRF

Component	Concentration (wt%)
MgO	0.71
$\text{Al}_2\text{O}_3$	1.81
$\text{SiO}_2$	46.10
$\text{P}_2\text{O}_5$	0.36
Br	0.80
$\text{TiO}_2$	50.08
$\text{Cr}_2\text{O}_3$	0.14



Fig. 1. FTIR spectrum of as-prepared  $\text{TiO}_2/\text{SiO}_2$  composite.

$\text{cm}^{-1}$  in spectrum. The band at around  $1100 \text{ cm}^{-1}$  can be assigned to  $\text{SiO}_2$  matrix, the band at around  $490 \text{ cm}^{-1}$  is representative of  $\text{TiO}_2$  matrix and the band at around  $950 \text{ cm}^{-1}$  has been assigned to the stretching of the  $\text{Si-O}^-$  species of  $\text{Si-O-Ti}$  [12]. Thus, the appearance of the band at around  $950 \text{ cm}^{-1}$  indicates that the titanium oxide species are embedded into  $\text{SiO}_2$  matrixes within these  $\text{TiO}_2/\text{SiO}_2$  nanocomposites.

The XRD patterns obtained for  $\text{TiO}_2/\text{SiO}_2$  nanocomposites are shown in Figure 2. According to Figure 2 as-synthesized  $\text{TiO}_2/\text{SiO}_2$  nanocomposite (TSR) without calcination is crystalline anatase phase in amorphous silica matrix. Amorphous silica transforms to cristobalite at  $950^\circ\text{C}$  but anatase phase is present in all of the synthesized composite samples up to  $1100^\circ\text{C}$ . The XRD patterns related to the TS400, TS600 and TS800 exhibit diffraction

lines attributed to brookite phase beside the anatase. The existence of brookite in XRD patterns is clearly evidenced from the presence of the (1 2 1) peak at  $2\theta = 30.81^\circ$  [4]. In samples prepared at higher calcination temperature, brookite phase disappeared. Both the interactions  $\text{Si-O-Ti}$  and this high dispersion prevent the crystalline transition to rutile [13] and only at very high temperature ( $1100^\circ\text{C}$ ), small peaks of rutile phase appears in the nanocomposite.

According to the Scherrer equation, the sizes of the anatase crystallites in the TSR, TS400, TS600, TS800, TS950, and TS1100 samples calculated to be 5, 5.09, 5.6, 7.8, 15.12, and 26.69 nm.

Differential scanning calorimetry and thermogravimetric curves of as-synthesized  $\text{TiO}_2/\text{SiO}_2$  composite (TSR) are shown in Figure 3.

The decrease in weight up to  $150^\circ\text{C}$  is



Fig. 2. XRD spectra of as-prepared  $\text{TiO}_2/\text{SiO}_2$  composite and samples heat-treated at different temperatures. (▲) peaks due to anatase, (□) peaks due to rutile, (■) peaks due to brookite, and (●) peaks due to  $\text{SiO}_2$  (cristobalite).

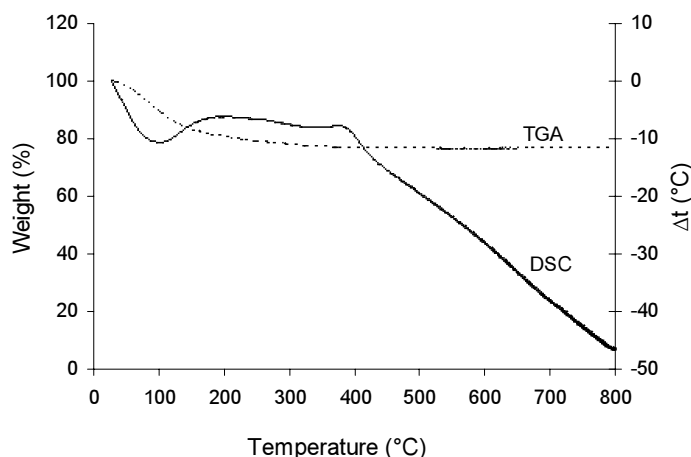


**Fig. 3.** TG-DSC curves for the as-prepared  $\text{TiO}_2/\text{SiO}_2$  nanocomposite (TSR).

attributed to desorption of physisorbed water and organic residue (confirmed by an endothermic peak on the DSC curve at about  $100^\circ\text{C}$ ). A diffuse exotherm at around  $400^\circ\text{C}$  is the result of the small portion of anatase crystallizing to brookite. Above  $400^\circ\text{C}$ , the change in weight is very small.

Figure 4. shows the typical TEM images of as-prepared  $\text{TiO}_2/\text{SiO}_2$  nanocomposite (TSR) and calcined sample at  $600^\circ\text{C}$ , also SEM image of calcined composite at  $1100^\circ\text{C}$ . The images show that all of composites have grainy structure and the particles size of the samples increases with increasing calcination temperature.

Figure 5. shows the absorption spectra (in the range 200–800 nm) of the RSR, TS800 and TS1100 samples dispersed in ethanol.

The band gap of the samples was calculated from the straight part of the optical absorption spectra using  $E_g = 1240/\lambda$  equation [14]. A clear red shift in the absorption edges of the composites is observed by increasing of calcination temperature. Band gap calculation of composites showed that the optical band gap of nanocomposites decreases ( $4.25\text{--}3.82\text{ eV}$ ) by increasing temperature to  $1100^\circ\text{C}$ . The shift can be ascribed to the difference in grain size of the samples. Zribi et al [15] have reported a similar trend with regard to optical band gap and temperature and suggested that the variation of density and the structural modifications may have caused the changes in the shape of the fundamental absorption edge. This spectral

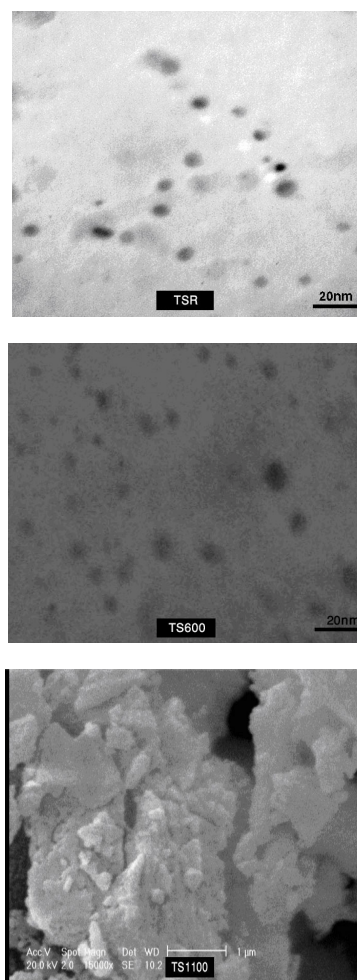


**Fig. 4.** TEM image of as-prepared composite (TSR) and composite prepared at  $600^\circ\text{C}$ , and SEM images of calcined composite at  $1100^\circ\text{C}$  (TS1100).

technique has also been employed to characterize the chemical nature and the coordination sphere of Ti ions incorporated into the silica matrix. Odenbrand et al [16] have shown that for coprecipitated silica–titania mixtures, isolated  $\text{SiO}_4$ -tetrahedra and exposed  $\text{Ti}^{4+}$ -tetrahedra were formed in mixtures consisting of amorphous silica and anatase phases. A peak corresponding to isolated Ti species which have absorption maxima at 210–225nm is observed in Figure 5. The absorption peak at 200–260 nm can be attributed to the charge transfer absorption process involving an electron transfer from the  $\text{O}_2^-$  to  $\text{Ti}^{4+}$  ions of the highly dispersed tetrahedrally coordinated  $\text{TiO}_4$  unit of the catalysts [17,18]. Anpo and co-workers have reported that titanium oxides having a tetrahedral coordination can be chemically supported onto silica matrix and have shown that such catalysts exhibit highly photocatalytic reactivities [18].

Figure 6. shows  $\text{N}_2$  adsorption-desorption

isotherms of TS400 and TS1100 composites. Detailed analysis showed that Isotherms of TS400, TS600 and TS800 are type IV and similar together.

For TS400, TS600 and TS800 the hysteresis loop is a H2 type with a triangular shape and a steep desorption branch. Such behavior was attributed to the pore connectivity effects [19].

For TS1100 composite, hysteresis loop is an H4 type. Type  $H_4$  loops feature parallel and almost horizontal branches and their occurrence has been attributed to adsorption-desorption in narrow slitlike pores [20].

The surface area of TSR, TS400, TS600, TS800 and TS1100 samples calculated from BET to be 707.6, 405.3, 362.4, 206.5 and 14.8  $\text{m}^2/\text{g}$ , respectively. The surface area decreases from 707.59 to 14.78  $\text{m}^2/\text{g}$  with increasing calcination temperature up to 1100°C. Decreasing the surface area upon calcination is due to increasing the size of particles and better crystallization of them. It was found that the higher calcination

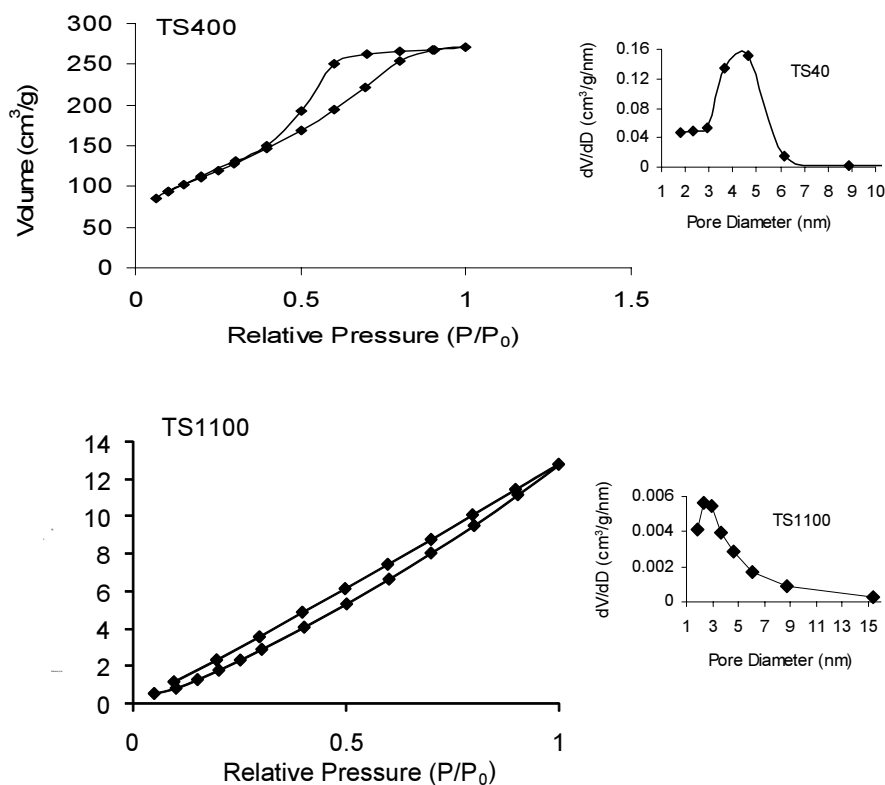


Fig. 3. TG-DSC curves for the as-prepared  $\text{TiO}_2/\text{SiO}_2$  nanocomposite (TSR).

temperatures led to better crystallinity, but usually decreased the surface areas of samples [21]. TS400, TS600, and TS800 composites possess a similar pore diameter that based on BJH plots obtained to be around 4.65 nm and pore diameter of TS1100 is 2.4 nm.

#### 4. DISCUSSION

A new free calcination sol-gel method was successfully used to prepare anatase  $\text{TiO}_2/\text{SiO}_2$  nanocomposite. Thermal phase transformation studies of the as-prepared composite were carried out to  $1100^\circ\text{C}$  by means of XRD and TGA-DSC analyses. In the non-thermal composite,  $\text{TiO}_2$  nanocrystals are dispersed in the amorphous  $\text{SiO}_2$  matrix. Formation of the Ti-O-Si bond and amorphous  $\text{SiO}_2$  in  $\text{TiO}_2/\text{SiO}_2$  could effectively increase the stability of anatase  $\text{TiO}_2$  which is a significant achievement regarding its possible photocatalytic applications. Anatase phase of  $\text{TiO}_2$  existed in all composites prepared at different temperatures. By heat treatment at  $400^\circ\text{C}$ , brookite phase was formed beside anatase phase. brookite  $\text{TiO}_2$  disappeared when calcination temperature exceeded to  $950^\circ\text{C}$ , and amorphous silica matrix was transformed to cristobalite. By increasing calcinations temperature to  $1100^\circ\text{C}$  small peaks of rutile phase were detectable at XRD pattern of composite sample.

It can be deduced from the results obtained that the calcination temperature governs on morphology, size and phase of the  $\text{TiO}_2$  nanoparticles dispersed in  $\text{SiO}_2$  matrix.

#### 5. ACKNOWLEDGMENTS

Support by Nuclear Science and Technology Research Institute and Tarbiat Modares University is greatly appreciated.

#### REFERENCES

1. Zhang, R., Ga, L., Zhang, Q., "Photodegradation of Surfactants on the Nanosized  $\text{TiO}_2$  Prepared by Hydrolysis of the Alkoxide Titanium" *Chemosphere*, 2004, 54, 405-411.
2. Richardon, S., Thruston, A., Collette, T., Patterson, K., Lykins, B., "Identification of  $\text{TiO}_2$ /UV disinfection byproducts in drinking water". *J. Ireland, Environ. Sci. Technol.*, 1996, 30, 3327-3334.
3. Fei, H., Liu, Y., Li, Y., Sun, P., Yuan, Z., Li, B., Ding, D., Chen, T., "Selective synthesis of borated meso-macroporous and mesoporous spherical  $\text{TiO}_2$  with high photocatalytic activity" *Microporous and Mesoporous Materials*, 2007, 102, 318-324.
4. Agatino, D. P., Giovanni, C., Maurizio, A., Marianna, B., Renzo, C., Marco, I., Riccardo, C., Leonardo, P., "Photocatalytic activity of nanocrystalline  $\text{TiO}_2$  (brookite, rutile and brookite-based) powders prepared by thermohydrolysis of  $\text{TiCl}_4$  in aqueous chloride solutions". *Colloid Surf. A: Physicochem. Eng. Asp.*, 2008, 317, 366-376.
5. Mills, A., Le Hunte, S., "An overview of semiconductor photocatalysis". *J. Photochem. Photobiol. A: Chem*, 1997, 108, 1-35.
6. Ovenstone, J., "preparation of novel titania photocatalysts with high activity". *Mater. Sci.*, 2001, 36, 1325-1329.
7. Janitabar-Darzi, S., Mahjoub, A., "Investigation of phase transformations and photocatalytic properties of sol-gel prepared nanostructured  $\text{ZnO}/\text{TiO}_2$  composites". *Journal of Alloys and Compounds*, 2009, 486, 805-808.
8. Reidy, D. J., Holms, J. D., Morris, M. A., "preparation of a highly thermally stable titania anatase phase by addition of mixed zirconia and silica dopants". *Ceram. Int.*, 2006, 32 (3), 235-239.
9. Tian, B., Chen, F., Zhang, J., Anpo, M., "Influences of acids and salts on the crystalline phase and morphology of  $\text{TiO}_2$  prepared under ultrasound irradiation". *Journal of Colloid and Interface Science*, 2006, 303, 142-148.
10. Yusuf, M. M., Imai, H., Hirashima, H., "preparation of porous titania film by modified sol-gel method and its application to photocatalyst". *J. Sol-Gel Sci. Technol*, 2002, 25, 65-74.
11. Stengl, V., Bakardjieva, S., Murafa, N., Vecernýkova, E., Subrt, J., Balek, V. "Preparation and characterization of titania based nanowires". *J Nanopart. Res.*, 2007, 9, 455-462.
12. Davis, R. J., Liu, Z., "Titania-Silica: A Model

- Binary Oxide Catalyst System". *Chem. Mater.*, 1997, 9, 2311–2324.
13. Aguado, J., Grieken, R., Lopez-Munoz, M., Marugan, J., "A comprehensive study of the synthesis, characterization and activity of  $\text{TiO}_2$  and mixed  $\text{TiO}_2/\text{SiO}_2$  photocatalysts". *App. Catal. A: Gen.*, 2006, 312, 202–212.
14. Kamalasanan, M.N., Chandra, S., "Sol-gel synthesis of ZnO thin films". *Thin Solid Films*, 1996, 288, 112–115.
15. Zribi, M., Kanzari, M., Rezig, B., "Structural, morphological and optical properties of thermal annealed TiO thin films". *Thin Solid Films*, 2008, 516, 1476–1479.
16. Odenbrand, C. U. I., Andersson, S. L. T., Andersson, L. A. H., Brandin, J. G. M. and Busca, G., "Characterization of silica-titania mixed oxides". *J. Catalysis*, 1990, 125, 541–553.
17. Yan, X., He, J., Evans, D. G., Zhu, Y., Duan, X., "Preparation, Characterization and Photocatalytic Activity of  $\text{TiO}_2$  Formed from a Mesoporous Precursor". *J. Porous Materials*, 2004, 11(3), 131–139.
18. Yamashita, H., Ichihashi, Y., Harada, M., Stewart, G., Fox, M.A., Anpo, M., "Photocatalytic Degradation of 1-Octanol on Anchored Titanium Oxide and on  $\text{TiO}_2$  Powder Catalysts". *J. Catal.*, 1996, 158, 97.
19. Liu, H., Zhang, L., Seaton, N. A., "Analysis of Sorption Hysteresis in Mesoporous Solids Using a Pore Network Model". *J. Colloid Interface Sci.*, 1993, 156, 285.
20. Kruk, M., Jaroniec, M., "Gas Adsorption Characterization of Ordered Organic -Inorganic Nanocomposite Materials". *Chem. Mater.*, 2001, 13 (10), 3169–3183.
21. Bi, A. J., Wu, L., Li, Z., Ding, Z., Wang, X., Fu, X., "facile microwave solvothermal process to synthesize  $\text{ZnWO}_4$  nanoparticles". *J. Alloys and Compd.*, 2009, 480, 684–688.